The effect of radio frequency plasma processing reactor circuitry on plasma characteristics

Shahid Rauf[a] and Mark J. Kushner[b]
Department of Electrical and Computer Engineering, University of Illinois, 1406 West Green Street, Urbana, Illinois 61801

(Received 20 November 1997; accepted for publication 12 February 1998)

Past experiments have demonstrated that details of the external electrical circuitry can strongly influence the performance of radio frequency (rf) plasma processing reactors. Seemingly minor changes in the circuit, such as changing cable lengths, can lead to significantly different plasma characteristics. To investigate these couplings, a plasma equipment model has been developed which consists of a linked reactor simulation and a circuit model. In this hierarchy the results of the reactor simulation are periodically used in the circuit model to construct a simple representation of the plasma consisting of sheaths and resistors which are connected to the external circuit. Voltages (dc, fundamental and harmonics) and currents at all electrodes and reactor surfaces are computed, and are then employed as boundary conditions for the plasma reactor simulation. The models were used to investigate the effects of operating conditions, reactor geometry and stray coupling on the electrical characteristics of asymmetric capacitively coupled rf discharges. It was found that nonlinear sheaths lead to voltages and currents that have significant amplitudes at higher harmonics. As a consequence, external circuits that may appear identical to the plasma at the fundamental frequency may produce different plasma characteristics. Since plasmas are generally nonlinear and the combined plasma and circuit impedance is usually reactive, it was found that the voltage (or power) at the supply is not simply related to the voltages on electrode surfaces which generate the plasma. © *1998 American Institute of Physics.* [S0021-8979(98)03910-3]

I. INTRODUCTION

Since radio frequency (rf) powered plasmas are generally nonlinear, their interaction with the circuitry of plasma processing reactors is not an easily predictable relationship. Past experiments have, for example, demonstrated that the use of different circuit components—which nevertheless have equivalent characteristics at the fundamental frequency—can produce quite varied plasma and electrical properties.[1] Seemingly small variances in external circuit parameters, such as changing the cable length between the matchbox and the reactor, also have been found to strongly influence plasma characteristics.[2]

The electrical characteristics of rf plasma processing reactors have been actively investigated in the past. These works have concentrated on measuring electrical parameters, comparing those parameters with simple circuit models and determining plasma characteristics from the electrical data.[3–9] Past theoretical studies have made use of the fact that the electrodynamic properties of capacitively coupled discharges are primarily determined by the characteristics of the sheaths, which have enabled a number of analytical sheath models to be developed.[10–14] The most extensive set of electrical measurements reported to date are for the Gaseous Electronics Conference reference cell (GECRC).[15] Early in these studies, a detailed comparison of electrical measurements from different research groups was made using the same reactor design but which differed in minor details with the circuitry.[15] The widely varying results highlighted the fact that significant differences in plasma characteristics can be obtained in similar reactors with different external circuit components. Later studies focused on the effect of using different power supplies and the addition of reactive gases on electrical characteristics.[1,16] Sobolewski[17] made multiple point measurements of currents and voltages in the GECRC, developed an equivalent circuit model of the plasma reactor using this data, and later developed a sheath model for an asymmetric discharge.[18] Miller and Riley[19] recently extended their sheath and circuit model to address high plasma density inductively coupled systems having rf biased substrates.

With the advent of real time control strategies for plasma processing reactors, which employ first principles models to determine actuator settings such as electrode voltage, accurate representations of the nonlinear coupling between circuit parameters and plasma characteristics are required.[20] To address these needs, and to more generally investigate the nonlinear relationship between circuitry and plasma properties in asymmetric rf discharges, a coupled circuit and two-dimensional plasma equipment model has been developed. Our studies have focused on the capacitively coupled GECRC for which extensive experimental data is available. We investigated the effect of gas pressure, applied voltage, electrode spacing, addition of reactive gases and stray coupling on the electrical and plasma characteristics. The results and

[a]Electronic mail: rauf@uigela.ece.uiuc.edu
[b]Electronic mail: mjk@uiuc.edu

trends, in general, agree well with experiments. Results from this investigation show that the nonlinearity of the sheaths leads to currents and voltages which have significant higher harmonic content. As a consequence, plasmas do not interact identically with external circuits that may merely be equivalent at the fundamental frequency. For example, exchanging the matching network with an equivalent one at the fundamental frequency was found to have a noticeable effect on the dc bias and plasma properties.

The circuit and plasma reactor model are described in Sec. II. The models are used to investigate plasma–circuit interactions in Sec. III. Concluding remarks are in Sec. IV.

II. DESCRIPTION OF THE CIRCUIT MODEL

In this section, we describe our model for the rf bias circuitry. Since straight-forward simultaneous simulation of the plasma and external circuitry is often impractical because of the large disparity in plasma and circuit time scales, our approach iteratively links a plasma equipment model and a circuit model. In this approach, we periodically construct a simple circuit representation of the plasma reactor using intermediate results during the plasma equipment simulation. The circuit model consists of a set of interconnected sheaths and resistors which are connected to the external circuitry. The resulting nonlinear circuit is simulated until steady-state conditions are obtained. The results from the steady-state circuit model are then used to update voltages (dc, fundamental and harmonics) at the reactor electrodes, which act as boundary conditions for the solution of Poisson's equation in the plasma equipment model. This procedure is iterated until both the plasma and external circuit parameters attain steady-state values.

The plasma simulation into which the circuit model was imbedded is the Hybrid Plasma Equipment Model (HPEM), a two-dimensional simulation developed at the University of Illinois.[21–23] Since the HPEM has been described previously in detail, only a short description is included here. The entire HPEM consists of three coupled modules. The Electromagnetic Module solves Maxwell's equations for inductively coupled electromagnetic fields and models the inductive coil circuitry. The Electron Energy Transport Module (EETM) accepts these fields and uses either a kinetic Monte Carlo simulation or solves the electron energy equation to generate electron transport coefficients and source functions for electron impact reactions. These values are passed to the Fluid Kinetics Module (FKM) which calculates the species densities and fluxes using the continuity and momentum conservation equations, and Poisson's equation is solved to provide the electrostatic fields. These values are passed to the other modules, and the process is iterated to convergence. The circuit model has been integrated into the FKM. As capacitively coupled reactors are being addressed in this study, only the EETM and the FKM have been employed. The Monte Carlo simulation option has been used for electron energy transport which captures all pertinent electron heating mechanisms, including anomalous sheath heating.[24]

The simplified circuit model for the plasma, shown in Fig. 1, consists of a set of interconnected sheaths at all important reactor surfaces. The bulk plasma is approximated by simple resistances. The sheaths are each connected to a series of external circuit elements terminating with a power supply. By choosing appropriate values for the circuit elements, and voltages for the power supply, most circuit and matchbox configurations of interest can be investigated. The sheath model we employed was originally developed by Metze, Ernie and Oskam (MEO).[10] The implementation, however, follows the procedure outlined by Riley.[14] For the circuit simulation, we treat the sheaths as nonlinear circuit elements for which the current–voltage relationship $V(I)$ is known. This relationship is obtained from the MEO model in terms of four parameters: electron density at the presheath–sheath interface n_o, electron temperature in the presheath T_e, ion velocity at the sheath–presheath interface v_i, and surface area of the electrode A. In the work of Miller and Riley[19] these parameters are provided by experimental measurements, whereas in this work the parameters are extracted from the HPEM, the details of which are explained below.

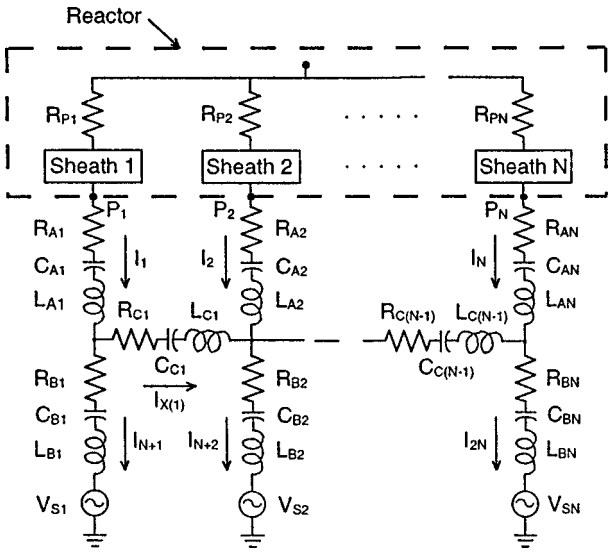

FIG. 1. A schematic of the general circuit model. The plasma processing reactor is approximated by a set of sheaths and resistors, where the component values are obtained from the plasma equipment model.

In the sheath model, electrons are assumed to obey the equilibrium Boltzmann distribution. Electron current in the sheath is, therefore,

$$I_{\text{elec}} = -\frac{n_o e}{4}\left(\frac{8k_B T_e}{\pi m}\right)^{1/2} \exp\left[\frac{eV}{k_B T_e}\right] A, \tag{1}$$

where e, m, k_B and $V(x,t)$ are, respectively, the electron charge, electron mass, Boltzmann constant and potential. Sheaths are assumed to be collisionless. Ion current is, therefore, conserved across the sheath and can be written as

$$I_{\text{ion}} = e n_o v_i A. \tag{2}$$

The electric field in the sheath, E, can be computed using Poisson's equation and is given by

$$E=\sqrt{\frac{2n_o k_B T_e}{\varepsilon_o}}\left[\left(1-\frac{2eV}{k_B T_e}\right)^{1/2}+\exp\left(\frac{eV}{k_B T_e}\right)-2\right]^{1/2}, \tag{3}$$

where ion density has been related to the potential using ion momentum and energy conservation. The electric field and potential have been assumed to be zero at the sheath–presheath interface. Making use of current continuity, the voltage drop across the sheath is

$$V(t)=V(0)+\frac{1}{A\varepsilon_o}\int_0^t\left(\frac{dE}{dV}\right)^1 (I-I_{\text{elec}}-I_{\text{ion}})\ dt, \tag{4}$$

which specifies the $V-I$ relationship for each sheath.

The bulk plasma in the circuit model is approximated by simple series resistances which take into account ohmic and stochastic heating. The resistance attached to each sheath is[25]

$$R_P=\frac{m}{Ae^2 n_o}\left[\nu_m l+\left(\frac{k_B T_e}{m}\right)^{1/2}\right], \tag{5}$$

where ν_m is the momentum transfer collision frequency which we obtain from the HPEM and l is a scale length representing the distance from the edge to the sheath to the center of the plasma.

The sheaths are connected to an external circuit which is general enough that most external components, cables and stray elements can be represented. The resulting nonlinear circuit is implicitly integrated in time using finite differencing until all voltages and currents attain steady-state conditions. The exact set of integro-differential equations that are solved to compute the sheath voltages $V_{\text{SH}(i)}$ and currents $I_i(t)$: $i=1,2,\ldots,(2N-1)$, where N is the number of sheaths, are the following:

$$\begin{aligned}
&V_{\text{SH}(i)}[I_i(t)]+(R_{P(i)}+R_{A(i)})I_i(t)+V_{CA(i)}(0)+\frac{1}{C_{A(i)}}\int_0^t I_i(t)\ dt+L_{A(i)}\frac{dI_i}{dt}+V_{S(i)}(t)+R_{B(i)}I_{i+N}(t)+V_{CB(i)}(0)\\
&\quad+\frac{1}{C_{B(i)}}\int_0^t I_{i+N}(t)\ dt+L_{B(i)}\frac{dI_{i+N}}{dt}\\
&=V_{\text{SH}(i+1)}[I_{i+1}(t)]+(R_{P(i+1)}+R_{A(i+1)})I_{i+1}(t)+V_{CA(i+1)}(0)+\frac{1}{C_{A(i+1)}}\int_0^t I_{i+1}(t)dt+L_{A(i+1)}\frac{dI_{i+1}}{dt}+V_{S(i+1)}(t)\\
&\quad+R_{B(i+1)}I_{i+N+1}(t)+V_{CB(i+1)}(0)+\frac{1}{C_{B(i+1)}}\int_0^t I_{i+N+1}(t)\ dt+L_{B(i+1)}\frac{dI_{i+N+1}}{dt}i, \quad i=1,2,\ldots,(N-1),
\end{aligned} \tag{6}$$

$$\sum_{i=1}^{N} I_i(t)=0 \tag{7}$$

$$\begin{aligned}
&V_{S(i)}(t)+R_{B(i)}I_{i+N}(t)+V_{CB(i)}(0)+\frac{1}{C_{B(i)}}\int_0^t I_{i+N}(t)\ dt+L_{B(i)}\frac{dI_{i+N}}{dt}\\
&=R_{C(i)}I_{X(i)}(t)+V_{CC(i)}(0)+\frac{1}{C_{C(i)}}\int_0^t I_{X(i)}(t)\ dt+L_{C(i)}\frac{dI_{X(i)}}{dt}+V_{S(i+1)}(t)+R_{B(i+1)}I_{i+N+1}(t)+V_{CB(i+1)}(0)\\
&\quad+\frac{1}{C_{B(i+1)}}\int_0^t I_{i+N+1}(t)\ dt+L_{B(i+1)}\frac{dI_{i+N+1}}{dt}, \quad i=1,2,\ldots,(N-1).
\end{aligned} \tag{8}$$

In Eqs. (6)–(8), $V_{\text{SH}(i)}$, $V_{CA(i)}(0)$, $V_{CB(i)}(0)$ and $V_{CC(i)}(0)$ are, respectively, the voltage drop across the sheath i and the initial voltage at capacitors $C_{A(i)}$, $C_{B(i)}$ and $C_{C(i)}$. The circuit elements R_A, C_A, L_A, R_B, C_B, L_B, R_C, C_C, and L_C and locations of I_i are defined in Fig. 1. The currents $I_{2N}(t)$ and $I_{X(i)}(t)$: $i=1,2,\ldots,(N-1)$ in Eqs. (6)–(8) can be computed in terms of $I_i(t)$: $i=1,2,\ldots,(2N-1)$ using Kirchoff's current law. Once the voltages and currents attain steady-state, the voltages (dc, fundamental and harmonics) at nodes P_i: $i=1,2,\ldots,N$ are computed and they are used as boundary conditions for the solution of Poisson's equation in the HPEM.

The plasma parameters required for the sheath models are obtained from the HPEM. These parameters are averaged over the surface area of the specified material which is in contact with the sheath. Depending on the reactor conditions, the sheath can be considerably thinner than a mesh cell (inductively coupled discharges) or several mesh cells thick (capacitively coupled discharges). To determine the location of the sheath–presheath interface at every mesh point along a surface, the location where the total ion density and electron density are within a few percent of each other is determined by progressively moving away from the surface. The required plasma parameters are then computed by interpolating between the last two mesh cells. If the sheath width is

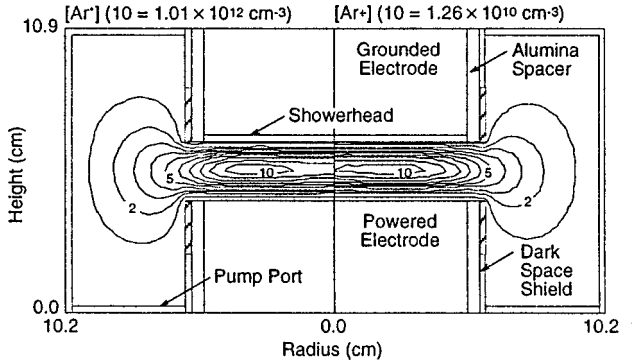

FIG. 2. Ar^+ and Ar* densities in the GECRC for Ar at 100 mTorr gas pressure, 100 V supply voltage and 10 sccm gas flow rate. The portions of the reactor for which wall current is collected are shown hatched.

smaller than a mesh cell, the values one mesh cell away from the electrode are used.

III. NONLINEAR CIRCUIT INTERACTION

In this section, results from the combined plasma equipment circuit model are described for the capacitively coupled GECRC. The motivating factor behind this choice of reactor is the extensive experimental electrical data that is available for the GECRC.[2,15–17] The geometry of the GECRC is shown in Fig. 2. The reactor has two parallel plate electrodes spaced 2.26 cm apart. The bottom electrode is powered and the top electrode is grounded. Gas flows in through a showerhead in the top electrode and it is pumped out at the bottom of the reactor. The densities of metastable Ar (Ar*) and Ar^+ ions in the reactor are also shown in Fig. 2 for pure Ar at 100 mTorr gas pressure, 100 V (amplitude) applied voltage and 10 sccm gas flow. This particular simulation will be referred to as the standard case.

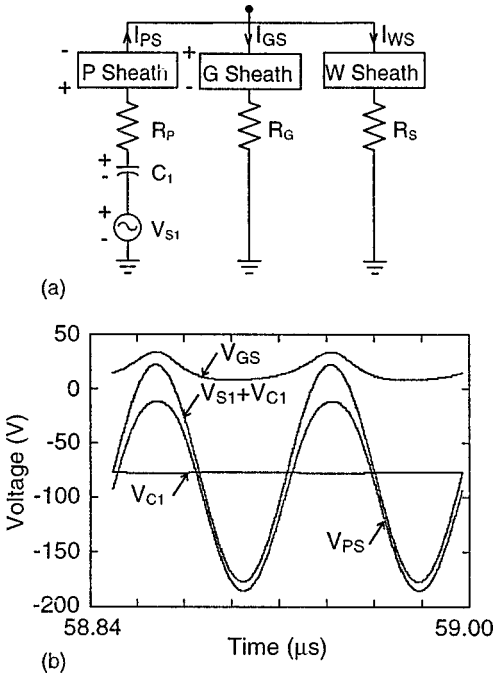

FIG. 3. Circuit parameters for a three-surface, three-sheath model. (a) The simplified circuit model for the GECRC. *P*, *G*, *W* denote powered electrode, grounded electrode and wall sheaths. $C_1 = 300$ nF in this simulation, although the dc bias amplitude is not sensitive to the value of the blocking capacitance. (b) The steady-state blocking capacitor voltage (V_{C1}), sheath voltages (V_{GS} = grounded sheath, V_{PS} = powered sheath) and voltage at powered electrode ($V_{S1}+V_{C1}$) for the standard case.

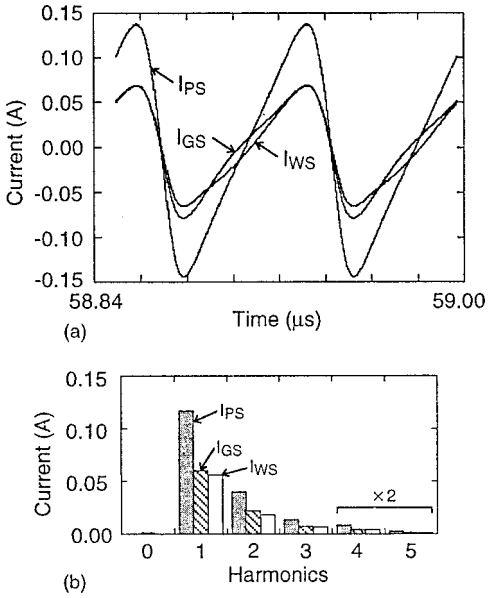

FIG. 4. Current parameters for the standard case. (a) Currents for the powered sheath (I_{PS}), grounded sheath (I_{GS}) and wall sheath (I_{WS}). (b) Harmonic content of the steady-state sheath currents.

In the first set of results, only a blocking capacitor and rf supply are connected to the powered electrode. For the circuit simulation, the reactor was divided into three surfaces each with its own sheath, as shown in Fig. 3(a). The first surface is the powered electrode, the second is the grounded electrode and the third constitutes the dark space shield which is also connected to ground. (Since the plasma density is low near the outside chamber walls, little current flows through the walls and they have been neglected in the circuit model. Simulations were performed including the outer walls as a fourth surface, and the results are essentially the same as the three-surface circuit.) The third surface consists only of portions of the dark space shield which are close to the plasma region (shown cross hatched in Fig. 2). We confirmed that negligible current flowed through the remaining portion of the dark space shield. To save computation time, we also lumped together the sheaths at the top and bottom dark space shields. The resulting steady-state sheath voltage drops and blocking capacitor voltage are plotted in Fig. 3(b) for the standard case. The corresponding sheath currents are shown in Fig. 4. To balance the ion and electron currents flowing through the grounded and powered surfaces, the blocking capacitor has charged to a negative voltage, the dc bias. The sheath voltages are characteristic of what one would expect in a capacitively coupled discharge.[25] The voltage at the powered electrode, $V_{S1}+V_{C1}$, is almost a shifted sinusoidal and has few significant higher harmonics. The currents through all the surfaces are, however, fairly nonlinear, and the second and third harmonics have significant amplitudes. The current that flows in through the powered elec-

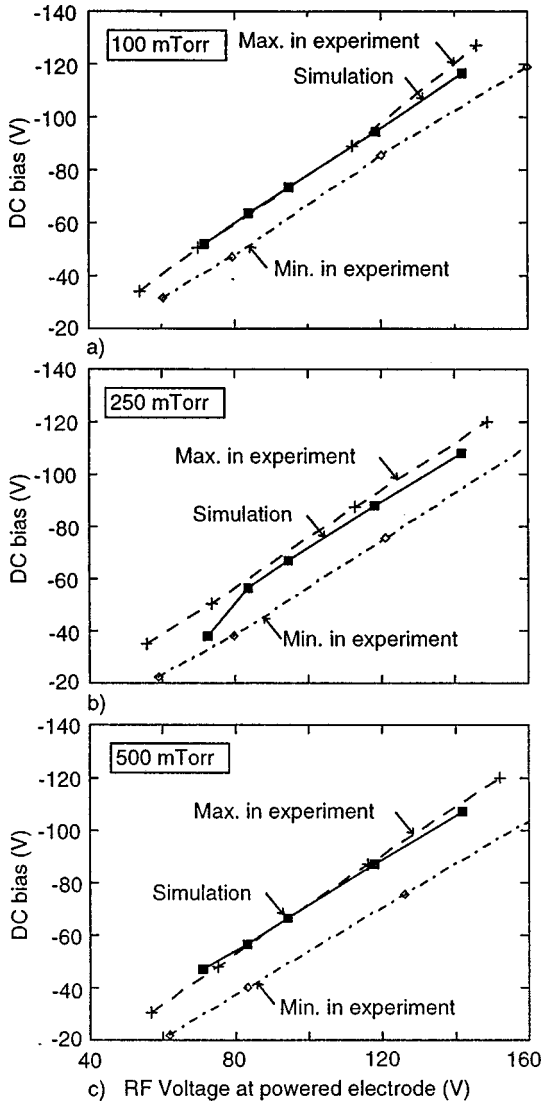

FIG. 5. dc bias in the GECRC for different supply voltages at (a) 100, (b) 250 and (c) 500 mTorr. The maximum and minimum ranges of the corresponding experimental data [Hargis *et al.*, Rev. Sci. Instrum. **65**, 140 (1994)] have also been plotted.

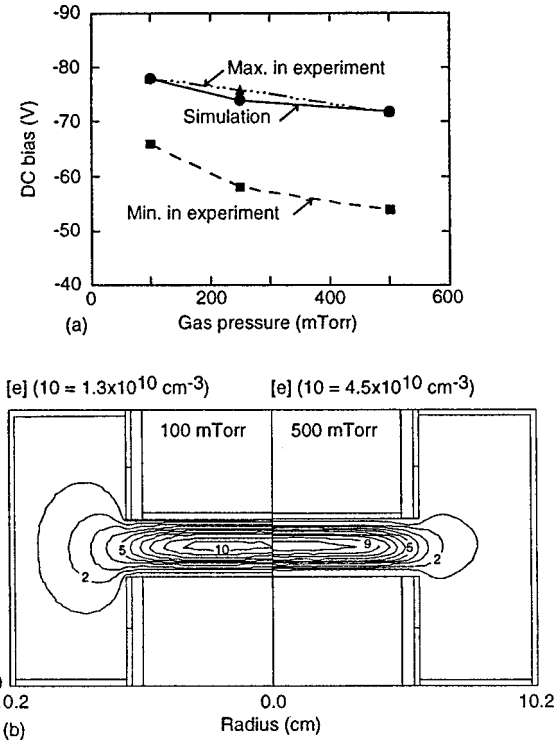

FIG. 6. Plasma characteristics as a function of pressure: (a) dc bias at 100 V applied voltage; (b) electron density at 100 and 500 mTorr. Decreasing pressure produces a more asymmetric discharge and a more negative dc bias.

trode divides almost equally between the grounded electrode and dark space shield under these conditions.

Using the same circuit as shown in Fig. 3(a), we varied the gas pressure and supply voltage. The resulting dc biases are shown in Fig. 5 along with the corresponding experimental data.[15] The limits of the experimental data in Fig. 5 are the minimum and maximum values obtained by a number of different research groups. The dc bias is plotted as a function of rf voltage amplitude at the powered electrode as opposed to the supply voltage. The results from the model agree well with the experiments throughout the range of pressures and rf voltages. At all pressures, the amplitude of the dc bias increases nearly linearly with applied rf voltage. Due to the asymmetrical nature of the $V-I$ characteristics of the two electrodes, as the applied voltage is increased, electron current increases more at the powered electrode than the grounded electrode. The dc bias voltage, therefore, increases to balance the two. At a given rf voltage, the magnitude of the dc bias decreases slightly as pressure is increased, as shown in Fig. 6. At higher pressures, the plasma is more tightly confined between the two electrodes with less current being collected by the dark space shield, as shown in Fig. 6(b). Since the discharge tends to become more symmetrical, the magnitude of the dc bias decreases.

The plasma model has been validated by comparison of two-dimensional Ar* and Ar^+ profiles to experimental results under similar conditions where both quantitative and systematic agreement were good.[26] For circuit parameters in additon to the dc bias, the model generally agrees well with experiments, although there are a few systematic discrepancies. For example, the magnitude and phase of the impedance of the sheath at the powered electrode and rf current flowing through it are compared to experiments for 100 mTorr in Fig. 7.[17] We find that the predicted impedance is slightly higher at low applied voltages, which results in lower than observed currents. The simulation results are, however, within 10%–20% of the experiments.

The impedance ($Z=R+iX$) of capacitively coupled discharges is highly reactive ($|X|\gg R$). For efficient power coupling, matching networks are often used inbetween the power supply (which tends to be resistive) and the reactor. Matching networks are LC circuits which can have several configurations. To illustrate the effects of the type of matching network on the plasma characteristics, we considered the two circuits shown in Fig. 8. All conditions are identical in the circuits except for the matching network. The network shown in Fig. 8(a) is a T-network, while that in Fig. 8(b) is a Π network. The component values were chosen such that the two matching networks are exact transforms of each other at

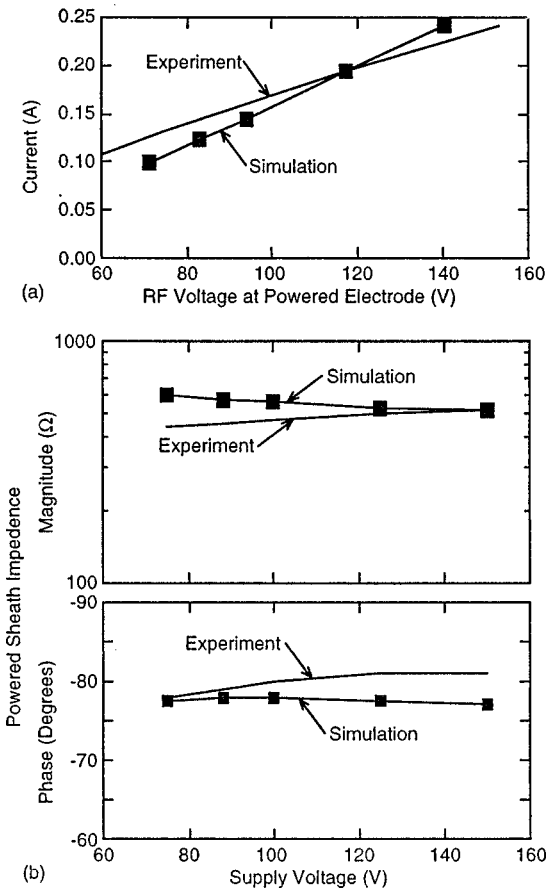

FIG. 7. Validation of predicted electrical characteristics. (a) rf current flowing through the powered electrode sheath as a function of rf voltage at powered electrode at 100 mTorr. Experimental results are from Hargis *et al.*, Rev. Sci. Instrum. **65**, 140 (1994). (b) Magnitude and phase of the impedance at the powered electrode sheath. Experimental results are from Sobolewski, IEEE Trans. Plasma Sci. **23**, 1006 (1995).

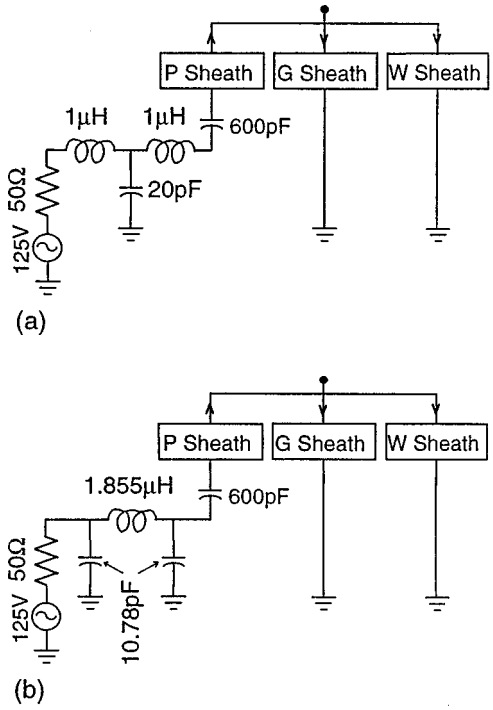

FIG. 8. Alternate matchbox circuits which are equivalent at the first harmonic. (a) T network, (b) Π network.

the fundamental frequency of 13.56 MHz. Plasma simulations were performed for both match boxes using operating conditions similar to those for the standard case. If the electrical character of the plasma was linear, the plasma's response to the two circuits would have been identical. The results from the simulation, however, showed that the dc biases obtained with the T and Π networks are different, -123.49 and -114.91 V, respectively for a supply voltage of 125 V. The dc bias develops due to the rectifying (nonlinear) nature of the sheaths. Although the two matching networks are equivalent at the fundamental frequency, they behave differently at other frequencies. For example, the Thevenin equivalent impedances of the two circuits at the second harmonic are $241.11 + i467.8\ \Omega$ and $259.43 + i663.56\ \Omega$. As a result the overall electrical characteristics, and in particular the dc bias, were different for the two circuits. The resulting plasma characteristics also were found to be different. For example, the peak electron densities with the T and Π networks were 3.76×10^{10} and 3.58×10^{10} cm^{-3}, respectively. The peak Ar* densities were 1.61×10^{12} and 1.51×10^{12} cm^{-3} for the T and Π networks. These results highlight the importance of not only properly modeling the external circuitry in rf plasma processing reactor simulations, but also being introspective about the impact that subtle circuit changes can have on electrical parameters used for real time control. Since our intention was to demonstrate that nonlinearity of the plasma causes rf plasma processing reactors to interact differently with different matching networks that might have identical characteristics at the fundamental frequency, no attempt was made to optimize the Π and T circuits separately.

In the T-circuit we used a supply voltage of 125 V. The first harmonic voltage at the powered electrode was 177.3 V. The plasma is highly capacitive while the matching network is inductive. Voltages at different nodes in the LC circuits can therefore be higher than the supply voltage, as we observed, due to resonant effects. The plasma conditions obtained for any given circuit depends on the voltages (dc, fundamental and harmonics) at the powered electrode which, unfortunately, are not related to the supply voltage in a simple manner since the plasma is nonlinear. For example, we ran another simulation in which the supply voltage for the T-circuit was decreased from 125 to 90 V. The dc bias and fundamental voltage decreased approximately by a factor of 1.39, which is essentially the same as the ratio of the supply voltages. However, the second and third harmonics decreased by 1.55 and 1.7 times, respectively. Since the harmonic content of the voltages at the electrodes depend not only on the external circuitry, but also on the absolute value of the input signal, the above results suggest that the voltage (or power) should be measured as close as possible to the electrodes.

As reactive and molecular gases are added to Ar, one would expect that the plasma conditions will change and there would be a commensurate change in the electrical characteristics. For example, we carried out simulations in which up to 5% N_2 was added to Ar. The pressure was kept con-

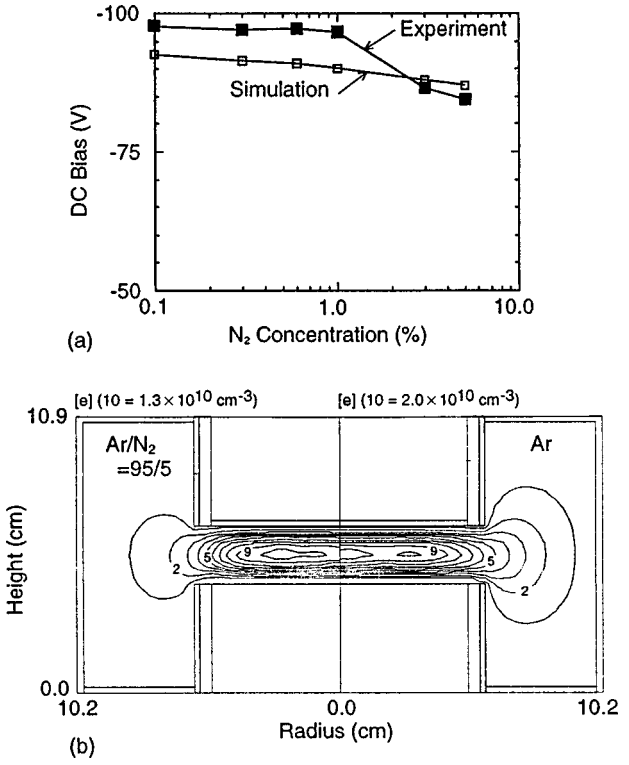

FIG. 9. Plasma characteristics for N_2 addition to Ar: (a) dc bias as a function of N_2 fraction, (b) electron density for 0.0 and 5.0% N_2. The gas pressure is 100 mTorr and the supply voltage is 125 V.

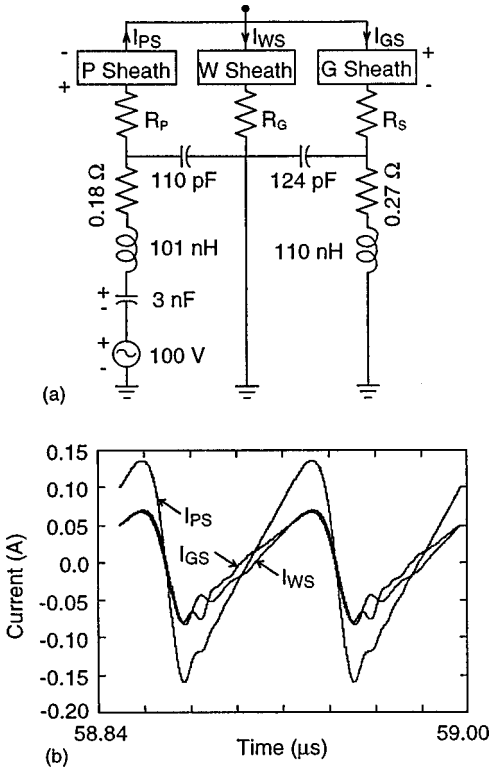

FIG. 11. Consequences of including parasitic circuit elements: (a) the simple circuit model with parasitic elements; (b) steady-state sheath currents.

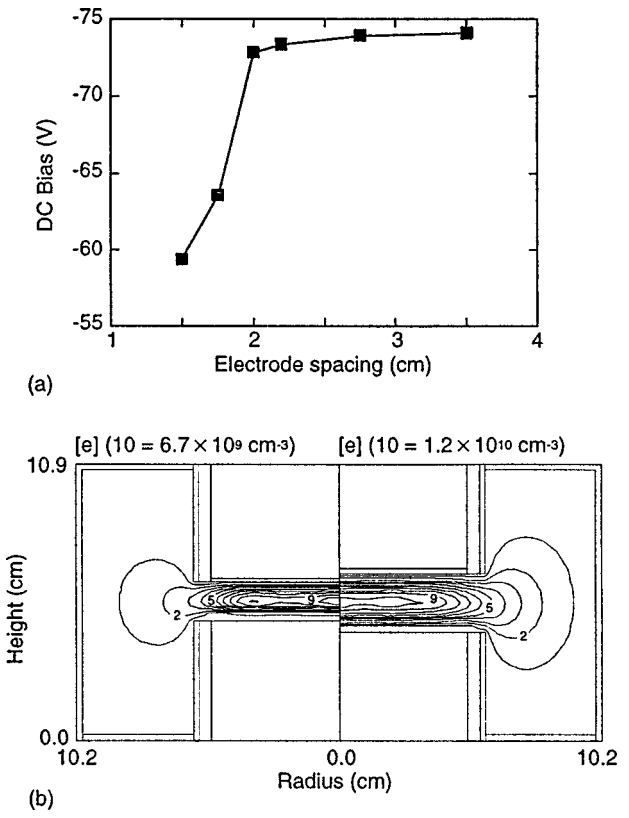

FIG. 10. Plasma characteristics for varying electrode spacings for the operating conditions of the standard case: (a) dc bias and (b) electron density for 1.5 and 2.25 cm electrode spacing.

stant at 100 mTorr and the supply voltage was 125 V. The resulting dc bias is shown in Fig. 9(a) with corresponding experimental data.[15] As N_2 is added, the plasma becomes more collisional as the inelastic electron mean free path decreases. This leads to a better confinement of the plasma in the inter-electrode region, as shown in Fig. 9(b), which produces more symmetrical operation and a decrease in the magnitude of the dc bias.

The GECRC is geometrically an asymmetric capacitively coupled discharge. The grounded reactor surface area is much larger than the powered electrode surface area, and a large dc bias is needed to balance the ion and electron currents through the electrodes. The actual dc bias ultimately depends on the relative axial and radial diffusivity of plasma. This dependence is shown in Fig. 10(a), where the dc bias is plotted as the electrode spacing is varied. All other dimensions of the reactor are kept constant. Conditions are similar to those for the standard case (100 mTorr, 100 V). As the two electrodes are brought closer together, a larger portion of the current from the powered electrode flows out through the grounded electrode. Since the surface areas of the two electrodes are equal, the discharge tends to become more symmetric as shown in Fig. 10(b), and consequently the dc bias amplitude decreases. As the electrode separation increases the dc bias saturates. In this regime, the grounded electrode is far enough from the powered one that a large portion of the current flows out through the dark space shield. At this point the discharge cannot become significantly more asymmetric, and the dc bias saturates close to the supply voltage.

Experimental current and voltage wave forms often have significant higher harmonic structure superimposed on the fundamental wave forms.[17] One factor that can contribute to these higher components is the stray resistance, capacitance and inductance of the circuit and the reactor. To demonstrate these effects, we added stray elements to the circuit of Fig. 3(a), producing the circuit shown in Fig. 11(a). The component values were obtained from Sobolewski.[17] Other than the changes in the external circuit, the simulation conditions were the same as those for the standard case. The currents flowing through the grounded, powered and wall sheaths are shown in Fig. 11(b). Comparing these values to the currents in Fig. 4(a), we find that the amplitude and relative distribution of current between the sheaths is essentially the same. The stray elements have, however, added higher harmonic structure to the wave form. Due to the nonlinear nature of the sheaths, the currents were rich in harmonic content even without the stray coupling. Some of the higher harmonics were resonantly amplified by the stray LC oscillators and the amplified harmonics added structure to the current wave forms in Fig. 11(b).

IV. CONCLUDING REMARKS

A combined plasma equipment model and circuit model have been applied to self-consistently investigate the interaction of plasmas in capacitively coupled discharges with their circuits. In the circuit model, the plasma reactor was approximated by a set of interconnected sheaths and resistors. The plasma equipment model provided sheath parameters (i.e., currents, densities, temperatures) and resistor values to the circuit model. These were used to compute the electrode voltages (dc, fundamental and harmonics), which were used as boundary conditions for the plasma equipment model. This procedure was iterated until both the plasma and circuit achieved steady-state.

We found that the resulting currents and voltages had significant magnitudes at higher harmonics due to the nonlinear nature of the sheaths. These nonlinear components complicate both the design of the external circuitry and interpretation of electrical data. External circuit components such as the blocking capacitor, power supply and matching network are generally linear. They will interact with each harmonic in a different manner. The plasma reactor will, therefore, not necessarily behave identically with different circuit components that may have identical properties at the fundamental frequency. This was demonstrated by considering two different matching network topologies that were equivalent at the fundamental frequency. The change of the matching network topology modified both the electrical and plasma characteristics. Plasma and circuit impedance are generally highly reactive. Voltages and currents may, therefore, vary nonmonotonically between the supply and electrodes. The plasma characteristics correspond to the particular set of voltages that appear at the electrodes and not to the supply voltage. Since the plasmas are nonlinear, the supply and electrode voltages are not related to each other in a simple manner. It is, therefore, best to measure the voltage as close as possible to the electrodes. We also investigated the effect of stray coupling. The stray LC oscillators were found to resonantly amplify some of the higher harmonics which added structure to the voltage and current wave forms.

ACKNOWLEDGMENTS

This work was supported by the National Institute of Standards and Technology, Air Force Office of Scientific Research (Grant No. F49620-95-1-0524), National Science Foundation (Grant Nos. ECS 94-04133, CTS 94-12565) and the Semiconductor Research Corporation.

[1] P. A. Miller, H. Anderson, and M. P. Splichal, J. Appl. Phys. **71**, 1171 (1992).
[2] M. A. Sobolewski, J. Res. Natl. Inst. Stand. Technol. **100**, 341 (1995).
[3] J. H. Keller and W. B. Pennebaker, IBM J. Res. Dev. **23**, 3 (1979).
[4] A. J. van Roosmalen, Appl. Phys. Lett. **42**, 416 (1983).
[5] A. J. van Roosmalen, W. G. M. van der Hoek, and H. Kalter, J. Appl. Phys. **58**, 653 (1983).
[6] P. Bletzinger and M. J. Flemming, J. Appl. Phys. **62**, 4688 (1987).
[7] P. Bletzinger, J. Appl. Phys. **67**, 130 (1990).
[8] C. Beneking, J. Appl. Phys. **68**, 4461 (1990).
[9] V. A. Godyak, R. B. Piejak, and M. Alexandrovich, IEEE Trans. Plasma Sci. **19**, 660 (1991).
[10] A. Metze, D. W. Ernie, and H. J. Oskam, J. Appl. Phys. **60**, 3081 (1986).
[11] M. A. Lieberman, IEEE Trans. Plasma Sci. **16**, 638 (1988).
[12] M. A. Lieberman, J. Appl. Phys. **65**, 4186 (1989).
[13] V. A. Godyak and N. Sternberg, Phys. Rev. A **42**, 2299 (1990).
[14] M. E. Riley, Sandia report SAND95-0775 (1995).
[15] P. J. Hargis, Jr., K. E. Greenberg, P. A. Miller, J. B. Gerardo, J. R. Torczynski, M. E. Riley, G. A. Hebner, J. R. Roberts, J. K. Olthoff, J. R. Whetstone, R. J. Van Brunt, M. A. Sobolewski, H. M. Anderson, M. P. Splichal, J. L. Mock, P. Bletzinger, A. Garscadden, R. A. Gottscho, G. Selwyn, M. Dalvie, J. E. Heidenreich, J. W. Butterbaugh, M. L. Brake, M. L. Passow, J. Pender, A. Lujan, M. E. Elta, D. B. Graves, H. H. Sawin, M. J. Kushner, J. T. Verdeyen, R. Horwath, and T. R. Turner, Rev. Sci. Instrum. **65**, 140 (1994).
[16] Special issue on the Gaseous Electronics Conference RF Reference Cell, J. Res. Natl. Inst. Stand. Technol. **100**, 327–494 (1995).
[17] M. A. Sobolewski, IEEE Trans. Plasma Sci. **23**, 1006 (1995).
[18] M. A. Sobolewski, Phys. Rev. E **56**, 1001 (1997).
[19] P. A. Miller and M. E. Riley, J. Appl. Phys. **82**, 3689 (1997).
[20] B. A. Rashap, M. Elta, H. Etemad, J. P. Fournier, J. S. Freudenberg, M. D. Giles, J. W. Grizzle, P. T. Kabamba, P. P. Khargonekar, S. Lafortune, S. M. Meerkov, J. R. Moyne, D. Teneketzis, and F. L. Terry, Jr., IEEE Trans. Semicond. Manuf. **8**, 286 (1995).
[21] P. L. G. Ventzek, R. J. Hoekstra, and M. J. Kushner, J. Vac. Sci. Technol. B **12**, 461 (1994).
[22] W. Z. Collison and M. J. Kushner, Appl. Phys. Lett. **68**, 903 (1996).
[23] M. J. Kushner, W. Z. Collison, M. J. Grapperhaus, J. P. Holland, and M. S. Barnes, J. Appl. Phys. **80**, 1337 (1996).
[24] M. Turner and M. B. Hopkins, Phys. Rev. Lett. **69**, 3511 (1992).
[25] A. Lieberman and A. J. Lichtenberg, *Principles of Plasma Discharges and Materials Processing* (Wiley, New York, 1994).
[26] S. Rauf and M. J. Kushner, J. Appl. Phys. **82**, 2805 (1997).